Electronic structure of anomalous muonium in GaP and GaAs

J. W. Schneider, K. Chow, R. F. Kiefl, S. R. Kreitzman, and A. MacFarlane
TRIUMF, Department of Physics, and Canadian Institute for Advanced Research, University of British Columbia, Vancouver, British Columbia, Canada V6T 2A3

R. C. DuVarney
Department of Physics, Emory University, Atlanta, Georgia 30322

T. L. Estle
Department of Physics, Rice University, Houston, Texas 77251

R. L. Lichti
Department of Physics, Texas Tech University, Lubbock, Texas 79409

C. Schwab
Centre de Recherches Nucléaires, F-67037 Strasbourg, France
(Received 27 October 1992)

The nuclear hyperfine structure of anomalous muonium in GaP has been resolved using muon level-crossing resonance. We find that 43% of the unpaired electron spin density resides on the nearest-neighbor Ga and 35% on the nearest-neighbor P on the ⟨111⟩ axis of symmetry. The *s* and *p* character of the unpaired spin density indicates that the Ga and P are displaced 0.23 and 0.54 Å away from the bond center. The now complete set of measured muon and nearest-neighbor nuclear hyperfine parameters for anomalous muonium in GaP and GaAs allows a detailed comparison of the two compounds, showing that the distribution of spin density among the group-III and group-V nearest neighbors in GaP is almost exactly the opposite of that in GaAs. This is contrary to what one would expect from a simple model of anomalous muonium in compound semiconductors involving an account of bonding characteristics.

I. INTRODUCTION

Hydrogen is important to our understanding of defects in crystalline semiconductors. An isolated hydrogen atom is the simplest interstitial impurity and is therefore of fundamental interest both to theorists and experimentalists. It has also been found recently that hydrogen passivates the electrical activity of shallow and deep acceptor and donor dopants in a wide variety of semiconductors.[1,2] Since hydrogen is present in many steps during the processing of Si or III-V devices, there is considerable additional motivation to understanding the microscopic properties of hydrogen, both in an isolated form and when it is complexed with the defect.

Most of our knowledge of isolated atomic hydrogen in semiconductors stems not from hydrogen itself, but from the light hydrogen "isotope" muonium (μ^+e^-), which can readily be studied with the technique of muon spin rotation (μSR).[3,4] These studies have shown that two types of muonium may be formed in many covalent semiconductors: "normal" muonium (Mu) with an isotropic hyperfine (hf) interaction with a magnitude of typically $\frac{2}{3}$ of A_0^μ, the value for Mu in vacuum, and "anomalous" muonium (Mu*) with a small anisotropic hf interaction of less than 10% of A_0^μ, with axial symmetry along a ⟨111⟩ crystalline axis.

Recently, there has been an enormous increase of structural information available on several of these muonium centers. Specifically, muon level-crossing resonance (μLCR) experiments, which probe the unpaired-electron spin density on the neighboring nuclei of muonium, have provided detailed and precise nuclear hf parameters for Mu* in Si (Ref. 5) and GaAs (Ref. 6) and for the two normal muonium centers (Mu^I and Mu^{II}) in CuCl.[7,8] As a result of the μLCR studies we now know that Mu* in Si and GaAs is muonium near the center of a covalent bond with unpaired-electron spin density primarily on the two nearest neighbors, which have relaxed appreciably away from the muon (bond-center model).

There have also been significant theoretical developments. Over the past few years, a number of *ab initio* calculations of the electronic structure and stability of hydrogen and muonium in elemental semiconductors[9–20] and III-V compounds[21–29] have been made. Van de Walle reported hf parameters for the muon and the first two shells of silicon atoms for Mu* in Si which were calculated using spin-density-functional theory, norm-conserving pseudopotentials, and a large-supercell geometry.[19] These results agreed with the μLCR determination of the hf parameters to within about 20%, even though the calculations did not allow for some important effects, such as the large μ^+ zero-point vibration.

 ©1993 The American Physical Society

Similar calculations are expected to be available soon on Mu* in GaAs (Ref. 29) and GaP.[30] For compound semiconductors it is important to evaluate the effect of ionicity on defect properties and on how well theory can explain them. For example, no Mu* centers have been observed in the more ionic (compared to GaAs and GaP) II-VI compounds.[3] In addition, the formation probability[31] of Mu* in GaP (Phillips ionicity: 32.8%[32]) is only about half that of Mu* in GaAs (Phillips ionicity: 31.0%[32]). Therefore a complete set of measured muon and nearest-neighbor hf parameters for GaP would allow such an evaluation for these two semiconductors. Independent of how successful theory may be in predicting nuclear hf parameters of Mu* in GaAs and GaP, a comparison of the experimental results for the two crystals could permit systematic trends to be detected.

We report here on a μLCR experiment that allowed us to resolve the nuclear hf structure of Mu* in GaP. Section II gives the theoretical background for interpreting μLCR spectra as well as for estimating nearest-neighbor relaxation from the measured hf parameters. Section III introduces the experimental setup; the measurements are described in Sec. IV; and in Sec. V the results are summarized and discussed, both in view of those for Mu* in GaAs and of theoretical work.

II. THEORY

A. μLCR

The spin Hamiltonian for Mu* and a neighboring nucleus n may be written as

$$\mathcal{H}=\mathcal{H}_{\mathrm{Mu}^*}+\mathcal{H}_n \ , \tag{1}$$

with

$$\mathcal{H}_{\mathrm{Mu}^*}=g_e\mu_B BS_{z'}-g_\mu\mu_\mu BI_{z'}+A^\mu_\parallel S_zI_z + A^\mu_\perp(S_xI_x+S_yI_y) \tag{2}$$

and

$$\mathcal{H}_n=-g_n\mu_n BJ_{z'}+A^n_\parallel S_zJ_z+A^n_\perp(S_xJ_x+S_yJ_y) +Q[J_z^2-\tfrac{1}{3}J(J+1)] \ . \tag{3}$$

$\mathcal{H}_{\mathrm{Mu}^*}$ is the Hamiltonian describing the hf interaction between the muon spin **I** and the electron spin **S** in a magnetic field **B** applied parallel to $\hat{z}'$, and $\mathcal{H}_n$ consists of additional terms involving the nuclear spin **J**. $A^\mu_\parallel$ and $A^\mu_\perp$ are the muon hf parameters, $A^n_\parallel$ and $A^n_\perp$ are the nuclear hf parameters, and Q is the nuclear electric quadrupole (NEQ) parameter. It is assumed that the hf and NEQ tensors are axially symmetric about a common axis $\hat{z}$, which is given by the muon-nucleus direction, and that the g tensors are isotropic. In our notation all g factors are positive, μ_B is the Bohr magneton, and μ_μ (μ_n) is the muon (nuclear) magneton. Note that because the μLCR's from one nucleus are effectively independent of other nonequivalent nuclei, it is sufficient to consider a spin Hamiltonian involving a single nucleus.[33]

The measured quantity in a μLCR experiment is proportional to the time-integrated muon spin polarization p parallel to both the applied field and the initial muon spin direction (see Sec. III). p is given by[34]

$$p=1-\frac{2}{N}\sum_{i,j>i}\frac{a_{ij}^2\omega_{ij}^2}{\lambda^2+\omega_{ij}^2} \ , \tag{4}$$

where $a_{ij}^2=|\langle\varepsilon_i|2I_{z'}|\varepsilon_j\rangle|^2$, $|\varepsilon_i\rangle$ is the ith energy eigenvector, $N=4(2J+1)$ is the dimension of the energy matrix, λ is the inverse muon lifetime, and $\hbar\omega_{ij}$ is the difference between the ith and jth energy eigenvalues. In high fields $[B\gg A^\mu_{\perp,\parallel}/(g_e\mu_B+g_\mu\mu_\mu)]$ and away from a μLCR, all a_{ij}'s in Eq. (4) are essentially zero, and hence $p(B)\simeq 1$. However, at certain fields B_r where the Larmor precession frequency ν_μ of the muon in the effective field matches that of a neighboring nucleus ν_n in *its* effective field, the two levels involved in the μLCR become mixed and the corresponding a_{ij} assumes a large value, leading to $p<1$ (Fig. 1). Therefore one expects a dip in the μLCR spectrum $p(B)$ at $B=B_r$. Approximate expressions for B_r for Mu* interacting with a spin-$\frac{3}{2}$ nucleus, valid in high fields and for small Q, are given by[33]

$$B_r=\frac{|A^\mu_\perp\mp A^n_\perp+(C^\mu\mp C^n)\cos^2\theta|\mp 2Q(3\cos^2\theta-1)k}{2(g_\mu\mu_\mu\mp g_n\mu_n)} \ , \tag{5}$$

where $C^i=A^i_\parallel-A^i_\perp$, θ is the angle between the symmetry axis of Mu* and the field, k assumes the values $-1,0,+1$, and the upper (lower) sign corresponds to a $\Delta=0$ ($\Delta=2$) resonance. Δ is defined by

$$\Delta=|m^\mu_{z'}(i)+m^n_{z'}(i)-m^\mu_{z'}(j)-m^n_{z'}(j)| \ , \tag{6}$$

where $m^\mu_{z'}$ and $m^n_{z'}$ are the eigenvalues of $I_{z'}$ and $J_{z'}$ and i and j refer to the two hf levels involved in the resonance

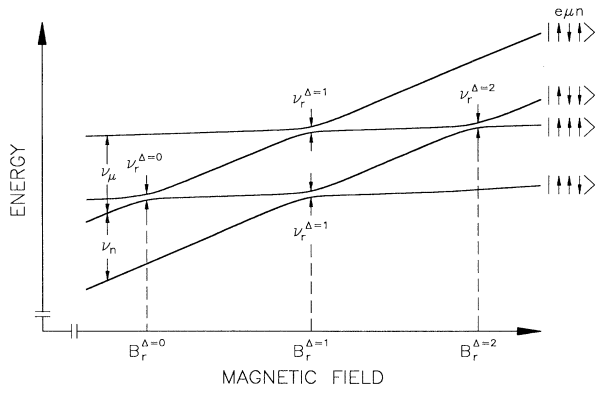

FIG. 1. Energy-level diagram of a paramagnetic system consisting of an electron (e), a muon (μ), and a single spin-$\frac{1}{2}$ nucleus (n). At specific fields B_r a part of the muon polarization oscillates with the "gap frequency" ν_r, causing a reduction in the time-integrated muon polarization ("level-crossing resonance"). The kets $|\uparrow\downarrow\uparrow\rangle=|m^e_{z'}=+\frac{1}{2},m^\mu_{z'}=-\frac{1}{2},m^n_{z'}=+\frac{1}{2}\rangle$, etc., indicate the approximate spin eigenstates of the system in a high magnetic field applied along z'. Δ is the absolute of the difference in $m^\mu_{z'}+m^n_{z'}$ between the hyperfine levels involved in a given resonance [see Eq. (6)].

(Fig. 1). At a $\Delta=0$ ($\Delta=2$) resonance, the muon and nuclear spins undergo a coherent oscillation with frequency ν_r defined in Fig. 1, with a phase difference of π (0), sometimes referred to as a "flip-flop" ("flip-flip") oscillation, that causes the reduction in the integrated muon polarization. In addition, there is in general a $\Delta=1$ resonance involving only the muon spin, at the field

$$B_r=\frac{|A_\perp^\mu+C^\mu\cos^2\theta|}{2g_\mu\mu_\mu} . \tag{7}$$

Finally, it will be useful to consider the result of an effective-field approximation,[35] valid in high magnetic fields, giving the two observable frequencies expected for Mu* in a high transverse field setup (see Sec. III):

$$h\nu^\pm=\tfrac{1}{2}[(C^\mu\sin\theta\cos\theta)^2 +(\mp 2g_\mu\mu_\mu B+A_\perp^\mu+C^\mu\cos^2\theta)^2]^{1/2} , \tag{8}$$

where the upper (lower) sign corresponds to a transition with the electron spin along (opposite to) the field direction.

B. Molecular orbitals

Consider the unpaired electron's wave function ψ for Mu* in a III-V compound. It can be approximated as a linear combination of normalized atomic valence orbitals centered on the muon and the nearest-neighbor group-III and group-V element:[36]

$$\psi=\eta_\mu\psi_\mu+\eta_{\rm III}\psi_{\rm III}+\eta_{\rm V}\psi_{\rm V} . \tag{9}$$

If overlap of the atomic orbitals is neglected, we get

$$\sum_i \eta_i^2=1 , \tag{10}$$

where the index i runs over μ, III, and V for the muon, the group-III element, or the group-V element. Hybridization is taken into account by decomposing each ψ_i into its s part α_i^2 and its p part β_i^2 according to

$$\psi_i=\alpha_i\psi_{s,i}+\beta_i\psi_{p,i} , \tag{11}$$

with

$$\alpha_i^2+\beta_i^2=1 , \tag{12}$$

since the ψ_i's are also normalized. Also, we decompose the hf interaction into a Fermi contact part A_s^i and a dipolar part A_p^i:

$$A_s^i=\tfrac{1}{3}(A_\parallel^i+2A_\perp^i), \quad A_p^i=\tfrac{1}{3}(A_\parallel^i-A_\perp^i) . \tag{13}$$

The hf parameters are related to the hybridization parameters α_i and β_i through

$$\eta_i^2\alpha_i^2=\frac{A_s^i}{A_{s,f}^i}, \quad \eta_i^2\beta_i^2=\frac{A_p^i}{A_{p,f}^i} , \tag{14}$$

where

$$A_{s,f}^i=\frac{8\pi}{3}\frac{\mu_0}{4\pi}g_e\mu_B g_i\mu_i\rho_{s,f}^i(0) ,$$
$$A_{p,f}^i=\frac{\mu_0}{4\pi}g_e\mu_B g_i\mu_i\int d^3r\,\rho_{p,f}^i(\mathbf{r})\frac{3\cos^2\alpha-1}{2r^3} \tag{15}$$

are the free atom values of A_s^i and A_p^i. $\mu_0=4\pi\times10^{-7}$ V s A^{-1} m^{-1} is the permeability of vacuum, $\rho_{s,f}^i(0)$ is the s spin density on i, $\rho_{p,f}^i(\mathbf{r})$ is the p spin density at position $\mathbf{r}$ with respect to i, and α is the angle between $\hat{z}$ and $\mathbf{r}$. Note that the s (p) spin density is equal to the square of the normalized valence s (p) wave function of i. The integral D in Eq. (15) can be reduced to

$$D=\tfrac{2}{5}\int_0^\infty\frac{P_r^2}{r^3}dr , \tag{16}$$

where P_r is the radial part of the valence p wave function of i. Calculated values of $A_{s,f}^i$ and $A_{p,f}^i$ for $i=^{31}$P, ^{69}Ga, and ^{75}As can be found in Ref. 37. We thus have a set of equations that allows an estimate of the wave-function parameters η_i, α_i, and β_i from the measured hf parameters.

C. Trigonal distortion of the nearest-neighbor bonds

The presence of Mu* causes a trigonal distortion of the four bonds of each nearest-neighbor atom along $\hat{z}$. The wave functions describing the four bonding orbitals may be written as

$$\psi_z=\alpha_z\psi_s+\beta_z\psi_{p_z} , \tag{17}$$

$$\psi_{\mathbf{a}}=\alpha\psi_s+\beta(a_x\psi_{p_x}+a_y\psi_{p_y}+a_z\psi_{p_z}) , \tag{18}$$

$$\psi_{\mathbf{b}}=\alpha\psi_s+\beta(b_x\psi_{p_x}+b_y\psi_{p_y}+b_z\psi_{p_z}) , \tag{19}$$

$$\psi_{\mathbf{c}}=\alpha\psi_s+\beta(c_x\psi_{p_x}+c_y\psi_{p_y}+c_z\psi_{p_z}) , \tag{20}$$

where **a**, **b**, and **c** are unit vectors pointing from a nearest neighbor towards the three next-nearest neighbors, θ_z is the angle between $\hat{z}$ and **a**, **b**, or **c**, and θ_{abc} is the angle between **a** and **b**, **b** and **c**, or **c** and **a** (Fig. 2). Requiring that the four wave functions be mutually orthogonal, we obtain

$$\cos\theta_z=-\frac{\alpha_z\alpha}{\beta_z\beta} \tag{21}$$

and

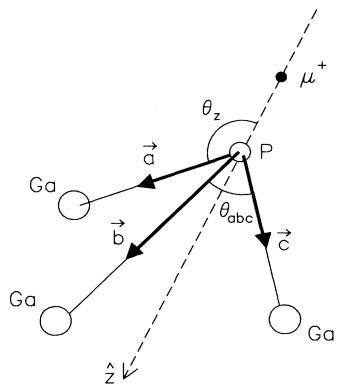

FIG. 2. The P nearest neighbor and the three Ga next-nearest neighbors of Mu* in GaP. Without Mu*, θ_z would be equal to the tetrahedral angle $\theta_t=109.5°$.

$$\cos\theta_{abc} = -\frac{\alpha^2}{\beta^2} \ . \tag{22}$$

From a straightforward geometrical consideration, one obtains

$$\cos\theta_{abc} = \tfrac{1}{2}(3\cos^2\theta_z - 1) \ . \tag{23}$$

Combining Eqs. (21)–(23) yields

$$\cos\theta_z = -\left[\frac{1}{2\dfrac{\beta_z^2}{\alpha_z^2}+3}\right]^{1/2} \ . \tag{24}$$

Note that by setting $\theta_z = \theta_{abc} = \theta_t$ in Eq. (23) we get $\cos\theta_t = -\frac{1}{3}$ and $\theta_t = 109.5°$, the tetragonal bond angle of the undistorted lattice. Setting $\theta_z = \theta_t$ in Eq. (24) yields $\beta_z^2/\alpha_z^2 = 3$, corresponding to a pure sp^3 hybrid orbital. By comparing θ_z with θ_t and assuming fixed next-nearest neighbors, one obtains for the relative displacement of the atom under consideration

$$\frac{\Delta b}{b} = \tfrac{1}{3}\{1 - 2/[(\beta_z^2/\alpha_z^2)+1]^{1/2}\} \ , \tag{25}$$

where b is the undistorted bond length.

D. Estimate of the spin-polarization effect

Ohta *et al.* performed an *ab initio* calculation of the hf constants of the radicals CH_3, SiH_3, and GeH_3.[38] These authors obtain the total spin density ρ_s from

$$\rho_s = \rho_{SD} + \rho_{SP} \ , \tag{26}$$

where ρ_{SD} arises from the delocalization of the radical orbital and is thus always positive or zero, while ρ_{SP} is due to the spin-polarization correction to the restricted Hartree-Fock wave function by the pseudo-orbital theory and can be positive or negative.[38] Using Eq. (15) to convert spin densities into hf parameters, Eq. (26) translates to

$$A_s^i = A_{SD}^i + A_{SP}^i \ . \tag{27}$$

Since the tabulated free-atom parameters $A_{s,f}^i$ do not contain a spin-polarization term, $A_{SD}^i = A_s^i - A_{SP}^i$ rather than A_s^i should be compared with $A_{s,f}^i$ in order to get an estimate of the "real" s atomic spin density $\eta^2\alpha_z^2(C)$,

$$\eta^2\alpha_z^2(C) = \frac{A_s^i - A_{SP}^i}{A_{s,f}^i} \ . \tag{28}$$

We can estimate A_{SP}^i for $i = {}^{69}\text{Ga}$, ${}^{75}\text{As}$, and ${}^{31}\text{P}$ using the tabulated ρ_{SP} values from Ref. 38 and Eq. (15).

III. EXPERIMENTAL DETAILS

The measurements were carried out at TRIUMF on beamlines M15 and M20, both of which provide intense beams [$(1-2)\times10^6$ μ^+/s] of low momentum (28.6 MeV/c), 100% backward spin-polarized positive muons. The GaP sample, an undoped single-crystal wafer with a carrier concentration of less than 3×10^{16} cm^{-3} and measuring 45 mm in diameter by 0.5 mm in thickness, was obtained from Hamaoka Toshiba Corporation, Japan. It was mounted in a He gas flow cryostat, where a constant temperature of 9 K was maintained throughout all measurements.

Figure 3 shows a schematic diagram of the center region of TRIUMF's HELIOS spectrometer. Note that such an arrangement of the positron telescopes [four forward ($F1-F4$) and four backward ($B1-B4$) counters, each covering $\pi/2$ of a cylindrical surface coaxial with the magnet axis] allows an easy changeover from a μLCR to a transverse-field setup. The spectrometer is shown in the μLCR mode with the forward positron telescope at position A. The measured quantity

$$s = \frac{\bar{B} - \bar{F}}{\bar{B} + \bar{F}} \ , \tag{29}$$

where

$$\bar{B} = B1 + B2 + B3 + B4 \ , \qquad \bar{F} = F1 + F2 + F3 + F4 \tag{30}$$

is a measure of p in Eq. (4). Bi and Fi are the total number of positrons counted by the respective detectors in the time interval defined by the total number of incoming muons one wants to accumulate per field point. Often it is advantageous to modulate s with a small flip field $\mathbf{B}_f$ with a magnitude of typically 5 mT, applied alternatively along and opposite to $\mathbf{B}$, to smooth out fluctuations in the

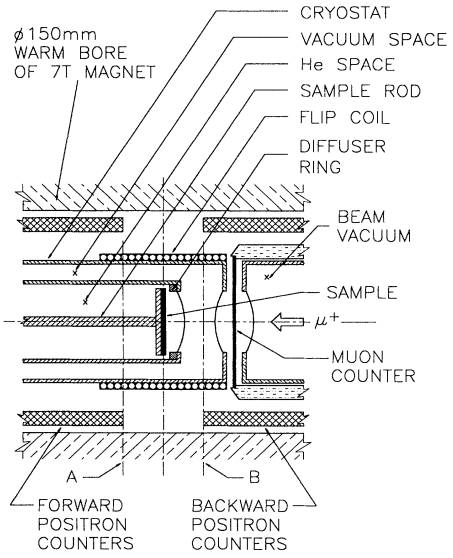

FIG. 3. Center region of the experimental setup inside the warm bore of the 7-T magnet. The incoming muons, whose spins are aligned antiparallel (perpendicular) to their momenta for a μLCR (transverse-field) experiment, are detected by the muon counter on entering the sample. In the μLCR mode shown here (forward positron counters in position A), the decay positrons are detected by the four forward and four backward counters, each of which covers $\pi/2$ of a cylindrical surface coaxial with the magnet axis. In transverse-field mode, only the forward positron counters, which are moved to position B, are used.

beam intensity which can cause steplike features in $s(B)$. In this case the measured quantity

$$s_m(B)=s(B+B_f)-s(B-B_f) \tag{31}$$

is usually called "asymmetry difference." In the transverse-field time-differential mode, the spin of the incoming muons is set perpendicular to the muon momentum, and the forward positron telescope is moved over the sample to position B in Fig. 3. In this case, four μSR time spectra are collected, one for each forward positron counter.

IV. MEASUREMENTS

From Eq. (5) it is clear that in order to determine the nuclear hf constants $A_{\parallel}^{n}$ and $A_{\perp}^{n}$ (the muon hf constants are assumed to be known), μLCR spectra containing resonances due to at least two different orientations of the symmetry axis of Mu* with respect to the field have to be taken. A typical procedure, which was also used in the present case, is to take a μLCR spectrum with a $\langle 110 \rangle$ axis along the field at one point during the experiment, which contains resonances for which $\theta=90°$ and $\theta=35.3°$. The position of the 90° resonances determines $A_{\perp}^{n}$ directly [Eq. (5)]. $A_{\parallel}^{n}$ can then be obtained from any other group of resonances caused by the same nucleus and for which θ is known.

If the sample is mounted with a $\langle 100 \rangle$ axis aligned with the field, as it was in the first part of the experiment, all four $\langle 111 \rangle$ axes form the same angle with the field. If, on the other hand, there is a small misalignment, one expects four slightly different angles θ and hence four times the number of resonances compared to the aligned case [Eqs. (5) and (7)]. This would be undesirable because it would (a) make the interpretation of the spectra more difficult and (b) prevent an accurate determination of the nuclear hf parameters.

Equation (8) implies that it is possible to align a crystal in which Mu* is formed using transverse-field μSR. Figure 4 shows μSR frequency spectra taken at $B=1$ T during the alignment of a $\langle 100 \rangle$ axis parallel to the field. All lines shown correspond to ν^{+} in Eq. (8). At the beginning, the sample was coarsely aligned, with two $\langle 111 \rangle$ axes in the horizontal plane and the other two in the vertical plane (a). The two outer (inner) lines are from Mu* states with their symmetry axes parallel to the two $\langle 111 \rangle$ axes in the horizontal (vertical) plane (the sample was deliberately misaligned by a few degrees in the horizontal plane). In (b) the sample is aligned in the vertical plane, and (c) shows an intermediate step of the alignment in the horizontal plane. (d) shows the final alignment where all four $\langle 111 \rangle$ axes form the same angle $\theta=54.7(3)°$ with the field.

The resulting μLCR resonances for ^{69}Ga are shown in Fig. 5(a). As expected from Eq. (5), the spectrum is particularly simple in this case, consisting of one triplet for $\Delta=0$ and one for $\Delta=2$. The solid line is an exact numerical calculation of a μLCR spectrum [Eqs. (4) and (31)], using the parameters given in Table I.

In the second part of the experiment, the sample was aligned with a $\langle 110 \rangle$ axis parallel to the field. A part of

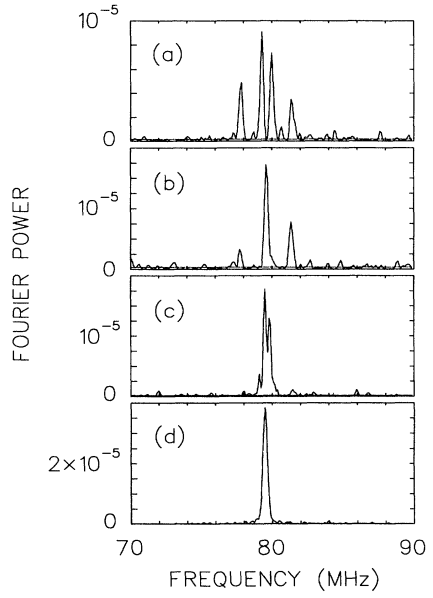

FIG. 4. Alignment of the GaP sample with a $\langle 100 \rangle$ axis parallel to the applied magnetic field of 1 T using transverse-field time-differential μSR. (a) shows the starting point where each of the four crystalline $\langle 111 \rangle$ axes is at a slightly different angle with the field, giving rise to four distinct μSR frequencies [ν^{+} in Eq. (8)]. In (b) the two $\langle 111 \rangle$ axes in the vertical plane are aligned, and (c) shows the alignment of the two $\langle 111 \rangle$ axes in the horizontal plane. In the final alignment (d) all four $\langle 111 \rangle$ axes form the same angle $\theta=54.7(3)°$ with the field. The sample temperature was 9 K.

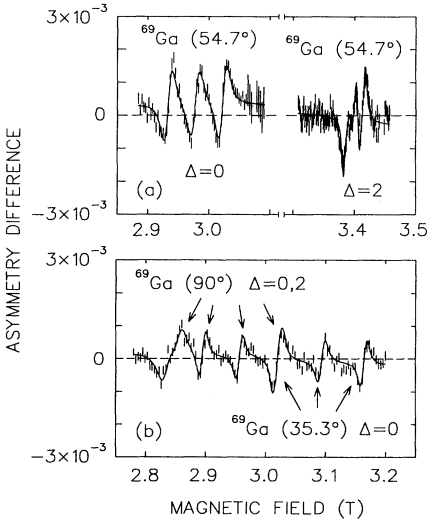

FIG. 5. Measured μLCR spectra of Mu* in GaP for $\langle 100 \rangle \| \mathbf{B}$ (a) and $\langle 110 \rangle \| \mathbf{B}$ (b) at a temperature of 9 K. θ, the angle between the symmetry axis of Mu* and the magnetic field, is given in parentheses for each group of resonances. Also indicated is the type of resonance Δ [Eq. (6)]. The solid lines are from an exact numerical calculation using Eqs. (4) and (31) and the parameters given in Table I.

TABLE I. Measured hyperfine and nuclear electric quadrupole parameters for Mu* and its nearest neighbors in GaP and GaAs and the s and p atomic spin densities obtained from $\eta^2\alpha_z^2=\frac{1}{3}(A_\parallel+2A_\perp)/A_{s,f}$ and $\eta^2\beta_z^2=\frac{1}{3}(A_\parallel-A_\perp)/A_{p,f}$. The free atom values $A_{s,f}$ and $A_{p,f}$ are from Morton and Preston (Ref. 37). $\eta^2\alpha_z^2(C)$ is the spin-polarization-corrected value of $\eta^2\alpha_z^2$.

Compound	Nucleus	$A_\parallel/h$ (MHz)	$A_\perp/h$ (MHz)	Q/h (MHz)	$\eta^2\alpha_z^2$	$\eta^2\beta_z^2$	$\eta^2\alpha_z^2(C)$
GaP	μ^+	219.0(2)[a]	79.48(7)[a]		0.0282		
	^{69}Ga	1017.8(1)	787.4(1)	3.94(3)	0.0708	0.377	0.0538
	^{31}P	620.2(4)[b]	249.7(1)[b]		0.0280	0.337	0.0082
GaAs	μ^+	218.54(3)[c]	87.87(5)[c]		0.0294		
	^{69}Ga	1052(2)[c]	867.9(3)[c]	1.08(3)[c]	0.0761	0.301	0.0591
	^{75}As	563.1(4)[c]	128.4(2)[c]	18.8(2)[c]	0.0186	0.434	0.0086

[a]Reference 31.
[b]Reference 4.
[c]Reference 6.

the μLCR spectrum for this orientation is shown in Fig. 5(b). In addition, the following resonances were observed and used to determine the nuclear hf and NEQ parameters given in Table I: ^{71}Ga (90°) $\Delta=0,2$ at 3.6–3.8 T, ^{69}Ga (35.3°) $\Delta=2$ near 3.8 T, ^{71}Ga (35.3°) $\Delta=0$ near 4.2 T. Note that natural Ga is an isotope mixture, consisting of 60.2% ^{69}Ga (spin-$\frac{3}{2}$) and 39.8% ^{71}Ga (spin-$\frac{3}{2}$), while natural P is isotopically pure ^{31}P (spin-$\frac{1}{2}$). From Eqs. (5) and (15) it is clear that, in general, there will be a different group of resonances for each isotope of the same element.

V. RESULTS AND DISCUSSION

A. Comparison of GaP and GaAs

The hf, NEQ, and bond parameters for Mu* and its nearest neighbors in GaP and GaAs are summarized in Table I. Note that the combined spin density on the two nearest neighbors is about 80% in both III-V compounds. However, the fractions of the spin density on the group-III and group-V elements are almost exactly reversed: For GaP, there is about 43% on the group-III element and 35% on the group-V element, while for GaAs the corresponding numbers are 36% and 44%. This seems to be incompatible with a qualitative model for Mu* in compound semiconductors,[22,23] in which the distribution of spin density among the two nearest neighbors X_1 and X_2 is a result of two competing mechanisms: On one hand, H or muonium is predominantly bonded to the element X_i for which the bond (X_i-H) is the strongest, leaving the unpaired electron in an antibonding orbital with a large overlap with the other nearest neighbor. On the other hand, the relative stability of the electron in the nonbonding orbital, a measure of which is the Pauling electronegativity of the element with which the nonbonding orbital is overlapping, plays an important role. Table II lists the (X_i-H) bond strength and Pauling's electronegativity for X_i=Ga,As,P. Consider first GaAs. In Ref. 23, the experimental results are explained by stating that the (Ga-H) and (As-H) bond strengths are not much different, and that the higher electronegativity of As therefore leads to the observed distribution of spin density, with more on the group-V and less on the group-III neighbors. For GaP, the difference between the (X_1-H) and (X_2-H) bond strengths is even smaller than for GaAs, while the electronegativity of P is slightly higher than that of As. Therefore one would expect an even more pronounced excess of spin density on the group-V neighbor for GaP, contrary to the experimental findings.

The displacement of the nearest-neighbor atoms due to the presence of Mu* is determined by the ratio of p to s spin density [Eq. (25)]. For GaP, this ratio is about 7 for Ga and 41 for P, while for GaAs, it is 5 for Ga and 50 for As. The resulting lattice relaxation parameters are summarized in Table III. In both compounds, the bond containing Mu* is stretched by about 30%. In GaP, the Ga (P) nearest neighbor is displaced about 10% (23%) away from the muon. In GaAs, the corresponding numbers are 6% (24%) for Ga (As).

B. Comparison of experiment and theory

As indicated in Sec. I, the muon and nearest-neighbor hf parameters represent the most meaningful set of data which one can use to test an *ab initio* calculation. The reason for this is that in the experiment, these parameters can be determined directly and with high precision (see Table I). Until now, most theoretical works did not give hf parameters, but rather bond relaxations, the relative stability of the impurity at various sites, etc. Recently, however, Van de Walle and Pavesi performed state-of-the-art first-principles spin-density-functional calculations for neutral hydrogen or muonium in GaAs.[29] Their work is of special interest because they give explicit values for the muon and nearest-neighbor nuclear hf pa-

TABLE II. Bond strength (dissociation energy) of the (X-H) bond at 298 K (Ref. 39) and Pauling's electronegativity (Ref. 40) for X=Ga,As,P.

Parameter	Ga	As	P
(X-H) bond strength (eV)	2.8	3.6	3.1
Electronegativity	1.6	2.0	2.1

TABLE III. Bond relaxation parameters for the nearest-neighbor atoms of Mu* in GaP and GaAs. $\Delta b/b$ is the total bond relaxation obtained by adding the contributions from the group-III and the group-V atoms. The undistorted bond length b is 2.36 Å for GaP and 2.45 Å for GaAs. Δb_{III} (Δb_{V}) is the amount the group-III (group-V) atom has moved away from the bond center with respect to the unrelaxed position. The experimental parameters include a correction due to spin polarization. The errors are estimated from the differences between the values with and without spin polarization.

Compound	$\Delta b/b$ (%)	Δb_{III} (Å)	Δb_{V} (Å)	Reference
GaP	33(9)	0.23(7)	0.54(19)	experiment
	37			theory (Ref. 25)
GaAs	30(5)	0.15(7)	0.59(10)	experiment[a]
	40	0.31	0.66	theory (Refs. 26,28,29)
	35	0.53	0.32	theory (Ref. 23)
	42			theory (Ref. 21)

[a]Hyperfine parameters taken from Ref. 6.

rameters and because they used an analogous technique as for Si, where the theoretical hf parameters agreed well with experiment. Their results, given in pairs ($A_{\parallel}^{i}$, $A_{\perp}^{i}$) in MHz units, are muon: (172,73), ^{69}Ga: (1126,958), ^{75}As: (272,−25). Comparing these values with experiment (Table I), we find generally good agreement, with the exception of $A_{\perp}$ for ^{75}As. This discrepancy can be explained by the very small s spin density on this atom, which is obtained in the calculation as the difference between two large numbers.[29] In addition to the hf parameters, these authors give the bond relaxation parameters for the nearest neighbors, which are in reasonable agreement with experiment (Table III).

The only previous theoretical study giving hf parameters for Mu* in a III-V compound, a Hartree-Fock cluster calculation, is also for GaAs.[23,25] These authors find $A_{\parallel}^{\mu}=130$ MHz and $A_{\perp}^{\mu}=-35$ MHz, but they do not give values for the nuclear hf parameters. The obvious discrepancy between theory and experiment may stem from principal difficulties of Hartree-Fock-type calculations in yielding accurate hf parameters.[29] However, the qualitative picture of Mu* emerging from this work agrees well with the experimental findings: Figure 1 in Ref. 23 clearly indicates that most of the spin density is on the two nearest neighbors, with slightly more on the As than on the Ga. Also, the p-to-s ratio for the Ga and As atoms nearest the impurity is 3.8 and 50, in excellent agreement with experiment. The total bond relaxation given in this work is compatible with experiment, while the calculated individual contributions of the group-III and group-V atoms are not (Table III). However, since the experimental values for the nearest-neighbor relaxations have been obtained in an indirect way and since the theoretical values themselves must have large error bars (an estimate may be obtained by comparing the relaxed bond lengths given by the two groups), the discrepancy between theory and experiment is not serious.

Finally, there are two more theoretical results on the total bond relaxation: one on Mu* in GaAs (Ref. 21) and one on Mu* in GaP (Ref. 25) (see Table III). Note that the latter, which is from the only calculation on the electronic structure of bond-centered muonium or hydrogen in GaP so far, agrees well with the experimental value.

VI. CONCLUSIONS

In conclusion, we have determined the electronic structure of Mu* in GaP using μLCR. Specifically, we report precise nuclear hf parameters for the nearest-neighbor Ga and P atoms, allowing an estimate of the s and p spin density on Ga and P and of the displacement of each of these atoms due to the presence of Mu*. We find that 43% (35%) of the unpaired spin is on the closest Ga (P), both of which have moved away from the muon. This distribution of spin density, with more on the Ga and less on the P, is the reverse of what is found for GaAs and thus disagrees with the trends predicted by a qualitative model for Mu* in compound semiconductors. While no calculations of the hf parameters for atomic hydrogen or muonium in GaP have been performed so far, our findings nevertheless match the unique features expected from the bond-center model for Mu* in a III-V semiconductor.

ACKNOWLEDGMENTS

We thank K. Hoyle and C. Ballard for technical support and C. G. Van de Walle and L. Pavesi for sending us a copy of their recent work on hydrogen and muonium in GaAs. This work was supported by the Natural Sciences and Engineering Research Council of Canada. The research of T.L.E. was supported by Grant No. C-1048 of the Welch Foundation and Grant No. DMR-8917639 of the U.S. National Science Foundation. R.L.L. was supported by Grant No. D-1053 of the Welch Foundation and, together with C.S. and R.C.D., by a NATO Collaborative Research Grant. The work of J.W.S. was partially supported by the Swiss National Science Foundation.

[1] *Hydrogen in Semiconductors*, edited by J. I. Pankove and N. M. Johnson, Semiconductors and Semimetals Vol. 34 (Academic, Boston, 1991).

[2] S. J. Pearton, J. W. Corbett, and M. Stavola, *Hydrogen in Crystalline Semiconductors* (Springer, Berlin, 1992).

[3] B. D. Patterson, Rev. Mod. Phys. **60**, 69 (1988).

[4] R. F. Kiefl and T. L. Estle, in *Hydrogen in Semiconductors* (Ref. 1), p. 547.

[5] R. F. Kiefl, M. Celio, T. L. Estle, S. R. Kreitzman, G. M. Luke, T. M. Riseman, and E. J. Ansaldo, Phys. Rev. Lett. **60**, 224 (1988).

[6] R. F. Kiefl, M. Celio, T. L. Estle, G. M. Luke, S. R. Kreitzman, J. H. Brewer, D. R. Noakes, E. J. Ansaldo, and K. Nishiyama, Phys. Rev. Lett. **58**, 1780 (1987).

[7]J. W. Schneider, M. Celio, H. Keller, W. Kündig, W. Odermatt, B. Pümpin, I. M. Savić, H. Simmler, T. L. Estle, C. Schwab, R. F. Kiefl, and D. Renker, Phys. Rev. B **41**, 7254 (1990).

[8]J. W. Schneider, H. Keller, W. Odermatt, B. Pümpin, I. M. Savić, H. Simmler, S. A. Dodds, T. L. Estle, R. C. DuVarney, K. Chow, R. Kadono, R. F. Kiefl, Q. Li, T. M. Riseman, H. Zhou, R. L. Lichti, and C. Schwab, Hyperfine Interact. **64**, 543 (1990).

[9]T. L. Estle, S. Estreicher, and D. S. Marynick, Phys. Rev. Lett. **58**, 1547 (1987).

[10]S. Estreicher, Phys. Rev. B **36**, 9122 (1987).

[11]S. Estreicher, Phys. Rev. B **37**, 858 (1988).

[12]S. A. Kuten, V. I. Rapoport, A. V. Mudry, R. B. Gelfand, A. L. Pushkarchuk, and A. G. Ulyashin, Hyperfine Interact. **39**, 379 (1988).

[13]P. Deak, L. C. Snyder, and J. W. Corbett, Phys. Rev. B **37**, 6887 (1988).

[14]P. Deak, L. C. Snyder, J. L. Lindström, J. W. Corbett, S. J. Pearton, and A. J. Tavendale, Phys. Lett. A **126**, 427 (1988).

[15]G. G. DeLeo, M. J. Dorogi, and W. B. Fowler, Phys. Rev. B **38**, 7520 (1988).

[16]S. Vogel, M. Celio, Dj.M. Maric, and P. F. Meier, J. Phys. Condens. Matter **1**, 4729 (1989).

[17]C. G. Van de Walle, P. J. H. Denteneer, Y. Bar-Yam, and S. T. Pantelides, Phys. Rev. B **39**, 10 791 (1989).

[18]P. R. Briddon and R. Jones, Hyperfine Interact. **64**, 593 (1990).

[19]C. G. Van de Walle, Phys. Rev. Lett. **64**, 669 (1990).

[20]N. Paschedag, H. U. Suter, Dj.M. Maric, and P. F. Meier, Phys. Rev. Lett. **70**, 154 (1993).

[21]P. Briddon and R. Jones, in *Proceedings of the 3rd International Conference on Shallow Impurities in Semiconductors, Linköping, Sweden, 1988,* edited by B. Monemar, IOP Conf. Proc. No. 95 (Institute of Physics and Physical Society, London, 1988), 459.

[22]S. K. Estreicher, C. H. Chu, and D. S. Marynick, Phys. Rev. B **40**, 5739 (1989).

[23]Dj. M. Maric, S. Vogel, P. F. Meier, and S. K. Estreicher, Phys. Rev. B **40**, 8545 (1989).

[24]C. H. Chu and S. K. Estreicher, Phys. Rev. B **42**, 9486 (1990).

[25]Dj.M. Maric, S. Vogel, P. F. Meier, T. A. Claxton, and S. F. J. Cox, Hyperfine Interact. **64**, 567 (1990).

[26]L. Pavesi, P. Giannozzi, and F. K. Reinhart, Phys. Rev. B **42**, 1864 (1990).

[27]L. Pavesi and P. Giannozzi, Physica B **170**, 392 (1991).

[28]L. Pavesi and P. Giannozzi, Phys. Rev. B **46**, 4621 (1992).

[29]C. G. Van de Walle and L. Pavesi, Phys. Rev. B **47**, 4256 (1993).

[30]C. G. Van de Walle (private communication).

[31]R. F. Kiefl, J. W. Schneider, H. Keller, W. Kündig, W. Odermatt, B. D. Patterson, K. W. Blazey, T. L. Estle, and S. L. Rudaz, Phys. Rev. B **32**, 530 (1985).

[32]J. C. Phillips, in *Handbook on Semiconductors,* edited by T. S. Moss (North-Holland, Amsterdam, 1982), Vol. 1, Chap. 4C, p. 257.

[33]R. F. Kiefl, Hyperfine Interact. **32**, 707 (1986).

[34]J. W. Schneider, H. Keller, B. Schmid, K. Bösiger, W. Kündig, W. Odermatt, B. D. Patterson, B. Pümpin, H. Simmler, I. M. Savic, M. Heming, I. D. Reid, E. Roduner, and P. W. F. Louwrier, Phys. Lett. A **134**, 137 (1988).

[35]C. P. Slichter, *Principles of Magnetic Resonance* (Springer, Berlin, 1990).

[36]U. Kaufmann and J. Schneider, in *Festkörperprobleme: Advances in Solid State Physics,* edited by J. Treusch (Vieweg, Braunschweig, 1980), Vol. 20. p. 87.

[37]J. R. Morton and K. F. Preston, J. Magn. Reson. **30**, 577 (1978).

[38]K. Ohta, H. Nakatsuji, I. Maeda, and T. Yonezawa, Chem. Phys. **67**, 49 (1982).

[39]*Handbook of Chemistry and Physics,* edited by R. C. Weast (Chemical Rubber, Boca Raton, 1989).

[40]L. Pauling, *Nature of the Chemical Bond* (Cornell, New York, 1960).